Performance of the Recoil Mass Spectrometer and its Detector Systems at the Holifield Radioactive Ion Beam Facility

C. J. Gross [a,b,1], T. N. Ginter [c], D. Shapira [b], W. T. Milner [b], J. W. McConnell [b], A. N. James [d,e], J. W. Johnson [a,b], J. Mas [e], P. F. Mantica [a,2], R. L. Auble [b], J. J. Das [c,e,3], J. L. Blankenship [b,f], J. H. Hamilton [c], R. L. Robinson [b,4], Y. A. Akovali [b], C. Baktash [b], J. C. Batchelder [a], C. R. Bingham [b,f], M. J. Brinkman [b], H. K. Carter [a], R. A. Cunningham [g], T. Davinson [h], J. D. Fox [i], A. Galindo-Uribarri [b], R. Grzywacz [f], J. F. Liang [b], B. D. MacDonald [j], J. MacKenzie [h], S. D. Paul [b], A. Piechaczek [k], D. C. Radford [b], A. V. Ramayya [c], W. Reviol [f,5], D. Rudolph [b,6], K. Rykaczewski [b], K. S. Toth [b], W. Weintraub [f], C. Williams [a,b], P. J. Woods [h], C.-H. Yu [b], and E. F. Zganjar [k]

[a] *Oak Ridge Institute for Science and Education, Oak Ridge, Tennessee 37831 USA*

[b] *Physics Division, Oak Ridge National Laboratory, Oak Ridge, Tennessee 37831 USA*

[c] *Department of Physics and Astronomy, Vanderbilt University, Nashville, TN 37235 USA*

[d] *Department of Physics, University of Liverpool, P. O. Box 147, Liverpool L69 3BX, UK*

[e] *Joint Institute for Heavy Ion Research, Oak Ridge, Tennessee 37831 USA*

[f] *Department of Physics and Astronomy, University of Tennessee, Knoxville, TN 37996, USA*

[g] *CCLRC, Daresbury Laboratory, Warrington WA4 4AD, UK*

[h] *Department of Physics, University of Edinburgh, Edinburgh EH9 3JZ, UK*

[i] *Department of Physics, Florida State University, Tallahassee, Fl 32306, USA*

[j] *School of Physics, Georgia Institute of Technology, Atlanta, GA 30332, USA*

[k] *Department of Physics and Astronomy, Louisiana State University, Baton Rouge, LA 70803, USA*

Preprint submitted to Elsevier Preprint *8 December 1999*

Abstract

The recently commissioned Recoil Mass Spectrometer (RMS) at the Holifield Radioactive Ion Beam Facility (HRIBF) is described. Consisting of a momentum separator followed by an E-D-E Rochester-type mass spectrometer, the RMS is the centerpiece of the nuclear structure endstation at the HRIBF. Designed to transport ions with rigidities near K=100, the RMS has acceptances of $\pm$ 10% in energy and $\pm$ 4.9% in mass-to-charge ratio. Recent experimental results are used to illustrate the detection capabilities of the RMS, which is compatible with many detectors and devices.

Key words: Recoil Mass Spectrometer, gas detectors, moving tape collector, proton radioactivity, beta decay, gamma spectroscopy
PACS: 07.75.+h, 29.30.Aj, 29.30.Ep, 29.30.Kv, 29.40.Cs

1 Introduction

Our understanding of nuclear structure has been enhanced over the last decade through the expansion of in-beam γ-ray spectroscopic studies along the N=Z line [1–4], the explosion of work to delineate the proton drip line [5–9], and the identification of the excited states of proton-unbound nuclei [10–13]. Very neutron-deficient nuclei provide fertile testing grounds to discriminate between theoretical models [14–19] which usually are based on the nuclear structure observed closer to the valley of stability. However, many issues remain unresolved. Clear experimental evidence of neutron-proton pairing in the mid-mass nuclei has not been found. The effects of coupling to the nearby continuum in proton-unbound nuclei and changes to the underlying nuclear structure of these nuclei need to be explored. The properties of the ground and excited states of the nuclei along the path of the astrophysical rapid-proton capture process must be determined so that we can gain a better understanding of the rates which govern this process. These are just some of the projects where

[1] Corresponding author. Tel: +1-423-576-7698; Fax: +1-423-574-1268; email: cgross@mail.phy.ornl.gov.
[2] Present address: Department of Chemistry and NSCL, Michigan State University, East Lansing, MI 48824, USA
[3] On leave from Nuclear Science Center, Post Box 10502, New Delhi, India
[4] deceased
[5] Present address: Chemistry Department, Washington University, St. Louis, MO 63130, USA
[6] Present address: Department of Physics, Lund University, S-22100 Lund, Sweden

recoil mass spectrometers can be employed to learn valuable new nuclear structure information and its influence on the world around us.

Central to many of these studies has been the use of recoil mass spectrometers [20–24] in combination with new multi-detector arrays, such as double-sided silicon strip detectors (DSSD) [25], large Ge detector arrays [26–28], and highly-efficient, charged-particle detector arrays [29,30]. The keys to such studies is high detection efficiency and the suppression of background from reaction channels produced with many orders of magnitude larger cross-sections. A recoil mass spectrometer physically separates reaction products as a function of energy and mass-to-charge ratio (A/Q). Specific recoil products may be physically implanted into DSSDs or transported to a counting station via moving tape collectors (MTC). Detectors, such as DSSDs, use their high granularity and variable thickness to increase the effective number of detectors in a given area while reducing the count rates per effective detector. Gamma-ray spectroscopy typically uses the detection of multiple γ rays to discriminate between products produced with fusion-evaporation reactions and those produced with transfer and Coulomb excitation mechanisms. By correlating data from various detector systems located at the target and focal plane, enhancements in detection selectivity can be achieved such that nuclei produced and detected at a rate of a few events per day may be identified[5–8].

Even with these technical advances, there is a limit to the improvement of detection sensitivity since many reaction channels are open in a given compound nuclear reaction. Ultimately, the best suppression of the many "uninteresting" channels is achieved by not producing them. Through the use of radioactive ion beams (RIBs), the nuclei at the furthest edge of stability may be produced with sufficient absolute and relative total cross-section to be effectively studied. For example, the β-delayed protons following mass identification may be used to identify ^{125}Nd in the RIB reaction ^{58}Ni(^{69}As,pn)^{125}Nd. All similar reactions using stable beams will also produce much more of the β-delayed proton emitter ^{125}Ce, which hinders identification. However, RIBs also bring with them their own problems such as low intensity and a potentially high background caused by the radioactivity of the beam. Detection systems must be able to cope with this background problem. High granularity of detection systems coupled to a recoil mass spectrometer which has very good primary beam rejection is necessary to take advantage of the promise of RIBs. This article describes the Holifield Radioactive Ion Beam Facility's (HRIBF) nuclear structure endstation which is centered around the new Recoil Mass Spectrometer (RMS).

2 The HRIBF Recoil Mass Spectrometer

The HRIBF RMS is a spectrometer which combines a momentum separator with the traditional mass separator to provide superior primary beam rejection with highly efficient transport of reaction products. This spectrometer is able to be run with higher beam intensities using reactions with inverse kinematics than most other devices of its kind. The RMS, shown schematically in fig. 1, is designed to transport ions with magnetic rigidities up to $K = ME/Q^2 = 100$. The RMS contains seven quadrupoles, two sextupoles, three magnetic dipoles, and two electrostatic dipoles. Details of the optics and design criteria of the RMS may be found in refs. [31–33]. Initial commissioning results may be found in ref. [34] and the results of some early experiments may be found in ref. [35]. The spectrometer most similar to the RMS may be MARS [36] at Texas A&M which combines a momentum separator and a Wien filter.

The RMS has three focal planes: *(i)* the momentum dispersed focal plane inside quadrupole Q3, *(ii)* the achromatic focal plane after the momentum separator, and *(iii)* the A/Q dispersed focal plane at the end of the 25 m flight path. A further useful concentration of all the mass-separated products may be obtained after *(iii)* if the RMS is run in the converging mass mode solution discussed later. Unless otherwise designated, the term focal plane will refer to the A/Q focal plane *(iii)* at the end of the spectrometer.

2.1 Physical Description and Modes of Operation

The target position of the RMS, see fig. 2, is 75 cm away from the first (vertical focussing) quadrupole Q1. Provision has been made to accomodate a large Ge detector array (including GAMMASPHERE [28]) and other detectors with the RMS. The angular acceptance of the RMS is asymmetric with a designed horizontal acceptance of ± 30 mrad and vertical acceptance near ± 110 mrad. For comparison, the Daresbury Recoil Separator [21] (DRS) and Atlas Fragment Mass Analyzer (FMA) [22] are reported to have symmetric angular acceptances of approximately ± 45 mrad.

The first magnetic dipole D1 (together with Q1-Q2) results in a momentum-dispersed focus inside Q3. Here, a unique capability of the RMS is the ability to insert up to 7 thin rods, called fingers, to intercept the primary beam charge states which remain spatially well-defined. The transmission of reaction products from fusion-evaporations reactions should not be seriously degraded, as the products have a large distribution of momenta. The use of fingers is desirable when the beam has kinematic characteristics similar to the reaction products of interest, such as in strongly inverse-kinematic reactions. Figure 3 shows the results of an initial test of the fingers done by measuring the count rate of two charge states of the primary beam at the achromatic focus with, and without, fingers.

The second half of the momentum separator recombines the ions and focusses them at the achromatic focus. Quadrupole Q3 matches the energy dispersion caused by the two magnetic dipole sections. Sextupoles S1 and S2 are used to correct for higher order aberrations of the image at the focal plane. The image at the achromatic focus is typically a vertical bar more than 6 cm tall and 2 cm wide. The spatial distribution of ions at the achromatic focus is shown in fig. 4. Experiments not requiring mass identification may use this focal plane and reduce the time-of-flight between the target and recoil detectors. The beam profile may be changed to a more circular distribution from the bar shape which is present when the full RMS is used.

The mass separator is a separated electric-magnetic-electric field arrangement pioneered[20] at Rochester University. This particular combination of electric and magnetic fields, separating ions by energy and momentum, respectively, produces an A/Q dispersed image at the focal plane which has no dispersion in energy.

The focussing properties of the RMS can be varied to optimize different experimental conditions by adjusting subsets of elements together, a “knob” to produce a desired effect on the recoils with minimal impact on the other properties. For example, by adjusting a knob in the control program, the vertical focus of the final image can be varied from one centimeter to several without significantly impacting the transmission or dispersion of the device. A summary of all knobs currently available and their functions can be found in table 1.

In addition, the entire mode of operation of the RMS may be changed from the original diverging mass mode to the converging mass mode by switching the polarities of Q6 and Q7. In the diverging mode, masses move away from the optic axis after the final focal plane. The goal of the converging mass mode is to have an A/Q-dispersed focus at the focal plane detector with no significant loss in mass resolving power over the diverging mass mode, and have all masses converge into a single blob some 80 cm further down stream. The size of this blob is some 2-3 cm full-width at half-maximum (FWHM).

One property of the ion optics is that once a desired mode of operation is found for an ion travelling through the device, this mode may be extended to any ion simply by scaling the magnetic fields by the momentum-to-charge ratio and the electric fields by the energy-to-charge ratio. Thus, once the mode and any knobs are selected, the user needs only to supply the mass, energy, and charge state of the ion to be studied. To change the settings of the RMS, the theoretical GIOS [37] solution [31] is modified by any knob settings, scaled according to the mass, energy, and charge state of the desired ion, and adjusted to the actual RMS field values by the calibrations which we have determined experimentally. A flow diagram of the control logic is shown in fig. 5.

The ability to scale the components of the RMS by these simple algorithums permits the field settings of the RMS elements to be computer-controlled through the use of ADCs and DACs. All magnetic devices have Hall probes installed on a pole-surface, and the power supplies are adjusted until the correct fields are obtained. Magnetic dipoles are adjustable to within one part in 8000 (± 0.2 G) and all other magnetic elements are adjustable to one part in 800 (± 2 G). The electrostatic dipoles are monitored by current through a 6 GΩ resistor chain, and settings are controlled by 16-bit ADCs and DACs.

2.2 Commissioning and Performance

The RMS was commissioned by using an alpha source, accelerated beams from the 25-MV tandem, and products from fusion-evaporation reactions. Initially, a ^{244}Cm alpha source of several tens of μCi was placed on the optic axis at the achromatic focus and several E-D-E solutions were found which focussed the alpha particles onto the optic axis which coincided with the center of the position sensitive avalanche counter (PSAC) located at the focal plane. Each solution was then examined for steering of the alpha particles when the last two quadrupoles Q6-Q7 were energized. The solution which had produced no steering, *ie.*, ions were traveling along the optic axis through the quadrupole field regions, was chosen as a calibration point. The quadrupole doublet Q6-Q7 solution was set for the most tightly focussed image.

The alpha source was then moved to the target position (again on the optic axis) and a smaller PSAC was placed at the momentum focal plane inside Q3, and later, at the achromatic focus. In each case, the calibration points of the magnetic dipoles were taken as the field which directed the alpha particles to the center of the detector. The quadrupole doublets Q1-Q2 and Q4-Q5 were set to produce a double focus vertically and horizontally. The sextupoles and Q3 were not set during the tests with the alpha source.

After the initial calibrations were determined with the alpha source, the RMS was commissioned with a 110 MeV ^{32}S beam on a 300 μg/cm^2 target of ^{58}Ni and a 220 MeV ^{58}Ni beam on a ^{60}Ni target of 300 μg/cm^2. Initial settings were based on the results with the alpha source and with theoretical values used for quadrupole Q3 and the sextupoles. Mass separation was achieved from the very beginning. The knobs (including those involving the sextupoles) were used to obtain the optimum field values based on transmission and shape of the separated masses. Quadrupole Q3 was scaled individually based on the same criteria. New "best" values for each knob were determined and the knob coefficients were recalibrated such that knob values of 0 produce the expected optimized solution.

The final settings of the magnetic dipoles D1 and D2 were determined by using charge states of a 90 MeV ^{58}Ni beam passed through a carbon foil at the target position and physical interception of the ions along the optic axis. The first magnetic dipole field D1 was calibrated by finding the fields where charge states 12 and 25 were intercepted by a finger inside quadrupole Q3. The second magnetic dipole field D2 was calibrated by transporting the same charge states through 1 and 5 cm diameter collimators at the achromatic focus.

The final settings of the mass separator section of the RMS were obtained by using a fusion-evaporation reaction and an ionization chamber after the final focal plane. The electrostatic dipole ED1 was adjusted until there was no energy dependence observed in the mass position across the focal plane. Calculations with the ion-optics code GIOS [37] had suggested that the no-energy-dispersion condition depended most sensitively on this field setting. The magnetic dipole D3 and second electrostatic dipole ED2 were adjusted until the central ions were delivered to the optic axis with the appropriate A/Q acceptance. The image of the focal plane of the fusion evaporation reaction products from the ^{58}Ni + ^{60}Ni reaction is shown in fig 6. The mass resolution obtained from the projection of the recoils onto the horizontal (A/Q) axis is approximately $M/\Delta M = 450$.

This spectrum (fig. 6), taken in singles but with the requirement that four position signals be present, is dominated by reaction products, and there is very little evidence of scattered beam reaching the focal plane despite the symmetric kinematic reaction. Figure 6 also shows an example of primary beam suppression, provided by the RMS in the case of an inverse kinematic reaction. The low quantity of scattered beam reaching the focal plane of the RMS is expected to significantly reduce the background associated with radioactive ion beams and their decay products in focal plane experiments.

With the RMS operating in the diverging mass mode, a focal plane is produced which is independent of energy and is approximately 36 cm in length with a mass dispersion of $\sim$43 mm/%. The measured A/Q acceptance is $\pm$4.9% and the energy acceptance (FWHM) is approximately $\pm$10%. For comparison, the FMA [22] has an A/Q acceptance of $\pm$3.5% and an energy acceptance of $\pm$20%. The reduction in energy acceptance is a result of our larger (6 m bend radius) electrostatic dipole deflectors which, however, permit the acceptance of recoils with larger electric rigidities. In the converging mass mode, the mass resolution, A/Q acceptance, and energy acceptance are comparable with the diverging mode while compressing the physical size and separation of the masses by approximately a factor of two. In this mode all mass groups converge to a point some 80 cm from the PSAC along the optic axis. The spatial resolution of the ions at this point is poor and is on the order of 2-3 cm FWHM. The converging mass mode of operation may become the most common since detector sizes may be smaller, detector array geometries may be tighter, and higher detection efficiencies may be obtained by the convergence of multiple charge states of the same mass to one location.

2.3 Spectrometer Efficiency

The efficiency of a recoil mass spectrometer is dependent on many parameters including the physical construction, alignment, and design of the device. These things conspire to induce aberrations of second and higher orders which ultimately limit the ability of building a machine to transmit ions far removed from the central trajectory. Once a spectrometer is constructed and commissioned, the reaction kinematics, reaction channel, and target thickness dominate the ultimate performance of the device. For example, the mass resolution, transmission efficiency and beam rejection capabilities of a spectrometer, three often quoted measures of performance, are significantly different if one uses reactions such as C + Pb or Pb + C. Clearly, the Pb beam is more similar to the A≈220 reaction products than the C beam and will be transmitted further through the device. Thus, while the beam rejection may be poor for the Pb beam case, the kinematic focussing of such an inverse reaction ensures a high collection efficiency of recoil products with a narrow energy spread. Target thickness also plays a major role when discussing total efficiency of a device. In addition to multiple scattering degrading the mass resolution, a thick target will produce an energy distribution in the products which may fall outside spectrometer acceptance. In short, an infinitely thick target results in an efficiency of zero while an infinitely thin target produces an efficiency corresponding to the charge state distribution transmitted (neglecting losses from the evaporation process and charge exchange in the vacuum with residual gas). In practice, for a **production** target which is typically 300-1000 μg/cm^2, the efficiency of the RMS when using a symmetric reaction and detecting two charge states of a given mass is on the order of 5%.

Figure 7 contains data taken in $\gamma\gamma$ coincidence mode with and without the RMS. By gating on the γ-ray transition energy of 595 keV, γ rays corresponding to two reactions, ^{83}Y+3p and ^{80}Sr+α2p, are found. By determining the ratio of events in coincidence with the RMS, the overall detection efficiency of the RMS in these reactions may be measured. Note that they are different, presumably due to the larger recoil cone produced by evaporation of alpha particles.

2.4 Charge-reset Foils

The RMS target chamber allows the use of a charge reset foil approximately 10 cm from the target. Ions, as they leave the target, may lose their equilibrium charge state distribution if they have isomers which decay by internal electron conversion in a vacuum. It has been shown [38] that an ion which undergoes internal conversion may change charge state by as many as 5 units. The purpose of the reset foil, typically 20 μg/cm^2 carbon, is to reintroduce a charge state equilibium to the ions before they enter the RMS. The close proximity of the foil to the target makes this reset technique effective only for those ions with nanosecond isomers. A position further away from the target would result in mass resolution degradation due to multiple scattering and the resulting change in the trajectory of the ions as they pass through the foil.

The RMS uses two types of charge reset foil frames which are shown in fig. 8. A rectangular frame with 3 mm sides may be used in most experiments which do not depend on target area detector systems. The other frame is comprised of a thin tantalum strip of thickness 0.175 mm and width 1.75 mm. The strip is formed into a square shape approximately 30x30 mm^2 and results in a very small cross-section, which minimizes its ability to act as a catcher for Coulomb-scattered RIBs and as a blocker of charged-particle detectors placed at forward angles.

The large-area carbon foils, evaporated on glass slides, are floated onto warm distilled water dripped slowly into the vessel containing the slides. The foil is caught on the knife-edge of the frame and the water is heated and evaporated from the float container. Care must be taken to prevent bubbles from forming under the foil. These foils are extremely delicate and only about 50% survive the mounting process. A traditional type of frame is also available with a few millimeter-wide sides and has an area of 12.5x25 mm^2.

3 The Detectors of the RMS

Many detector systems and devices have been developed for use with the RMS and are listed in Table 2. These systems may be located at the target position and the various focal planes of the RMS. Working in combination with each other, the high selectivity required to study nuclei far from stability is achieved.

The focal plane detector is the Position Sensitive Avalanche Counter (PSAC) similar in design to the detector descibed in ref. [39]. This isobutane-filled gas detector is comprised of five wire planes which are separated by ~3 mm and has an active area of 36 x 10 cm^2. The wires are separated from each other by 1 mm, resulting in an overall transmission of approximately 90%. The physical arrangement with respect to the beam is cathode - horizontal (x) position - anode - vertical (y) position - cathode. The high voltage planes and x position plane are electrically segmented in half to reduce signal attentuation. Position is derived through time delay lines with adjacent pairs of wires leading to each tap of a 20 ns passive delay chip (2 ns per tap delay). Fast timing amplifiers and constant fraction discriminators are used, and ~2 mm position resolution (FWHM) has been measured by using an alpha source and a mask with 1-, 2,-, 3-, and 4-mm-diameter holes. Gas pressure is maintained at 3-4 Torr and voltages are set so that 40-50 mV (x200, ORTEC 820) amplified signals are present after passage through the 180 ns of the x delay line. The windows are made of commercially available Mylar^{TM} foils of 0.9 micron (~120μg/cm^2) thickness and are wire supported. Count rates of up to 10k have been sustained although efficiency suffers in local areas with high count rates. The loss appears to be caused by a lowering of signal gain either by depletion of the electrons within the gas and/or sparking resulting in deposits on the wires. Typically, the anode signals remain above disriminator thresholds indicating an ion has passed through the detector but the lower amplitude position signals do not cross the discriminator thresholds. "Holes" may appear in the focal plane spectrum as can be seen in fig. 9. In any case, higher gas flow or less-focussed ions can improve performance at high count rates. After use with high count rates, the wire planes may be rejuvenated by cleansing the wires with a soft sponge moisened with alcohol, suggesting that deposits are being formed.

A recent improvement to the focal plane has been the installation of three collimators for physically blocking the ions before reaching the PSAC. Presently, the focal plane has two side collimators on linear vacuum feedthroughs and one central collimator which can be lowered from above into position by a linear-rotating vacuum feedthrough. Although large enough to be used in either mode, these collimators have been primarily used with the converging mode so that only two charge states of one mass are transmitted to the focal plane detectors.

3.2 Ionization Chamber

A position-sensitive split-anode ionization chamber has been developed for HRIBF by Daresbury Laboratory and can be seen in fig. 10. The anode is split [40] along the direction of the beam into three segments of 58 mm, 50 mm, and 202 mm. The 8 mm of the first anode is placed over the reentrant window and provides a uniform electric field region inside the gas volume. Thus, the ionization for energy loss measurements is collected from two 50 mm anodes which may be added together. The total energy of the ions may be obtained by adding the signals from all three anodes. The ion chamber is also segmented horizontally into 8 sections of 51.5 mm so that in applications with localized, very high counting rates, pile-up and signal degradation can be minimized. These sections may be electrically bridged together to act as one. Our typical configuration is to split the ion chamber in half, as is done with the PSAC. The re-entrant mylar window has a 6 cm x 35 cm area and can be operated with up to 40 Torr of isobutane gas. The chamber has strip electrodes on the sides and back spaced at 5 mm intervals, and the window support wires have voltages applied to them to ensure perpendicular field gradients between the cathode and grids.

The cathode and Frisch grid are separated by 120 mm. A position-sense grid, which is held to ground through 200 kΩ resistors on either end of the delay line, lies between the Frisch grid and the anodes and is separated from each plane by 10 mm. Under operating conditions the voltages on the planes are: anode +8 V/Torr; position grid 0 V/Torr; Frisch grid -4V/torr; and cathode -28V/Torr.

The energy loss of ions has been measured with several fusion-evaporation reactions just above the Coulomb barrier. The data shown in fig 10 identifying transitions in ^{79}Y [4] reveal sufficient Z resolution in the energy-loss signals to differentiate neighboring isotopes at N = Z $\approx$ 40. In addition, γ rays from the neutron-deficient isotope, ^{125}Ce (Z=58) were identified with the ionization chamber by using the "centroid-shift" method [41].

3.3 Double-sided Silicon Strip Detectors

The double sided silicon strip detectors [25,42,43] currently in use at the HRIBF are 60 μm thick, 4 cm x 4 cm in size with 40 strips per side. One such detector, Micron Semiconductor Laboratory's BB/1, is shown in fig. 11. With this geometry the DSSD is comprised of 1600 pixels which act as individual silicon detectors. Two electronic circuits [42,43], provided by Edinburgh University, are used per strip: low gain amplifiers and leading-edge discriminators for high energy events such as implantation of the recoils and high gain amplifiers and leading-edge discriminators for lower energy events such as proton and alpha radioactivity following implantation.

Although implantation events usually overload the high gain circuitry the recovery time can be as short as 5 μs (7 μs is typical) and full energy decay events may be identified. Recently, ground state proton radioactivity in ^{145}Tm was measured[6] at the RMS with a half life of 3.5 (10) μs. After correction for pole zero effects, the energy of the proton was measured to be 1.728 (10) MeV, and the spectra are shown in fig 11. The thin profile of the DSSD to beta events, allow reaction products with sub-microbarn cross-sections to be studied. As is shown in fig. 11, a rare p5n evaporation channel was detected[8] with an estimated cross-section of 13 nb. All data presented here were taken in the diverging mass mode.

The DSSD is housed in a cube-shaped chamber with removable sides to provide maximum flexibility for various experimental conditions. A thick Si detector(s) may be placed immediately behind the DSSD to detect and distinguish between β events and β-delayed proton events which are not stopped inside the DSSD. Kevlar windows may be used with large planar X-ray detectors outside the vacuum system to provide element identification. Energy degrader foils and alpha calibration sources are also available within the vacuum chamber.

3.4 Moving Tape Collector

The Moving Tape Collector (MTC) was designed and built [44] for the HRIBF by Louisiana State University. The tape is aluminized 35 mm film approximately 30 m long, although lengths up to 50 m are supported. Transported by a stepper motor along sprockets and stored in a large box similar to a printer's ribbon cartridge, the tape may be moved at rates up to one meter per second. Connected to the focal plane of the RMS with quick-connect clamp flanges the path of the tape may vary according to the experimental conditions. In addition, the MTC can be operated in two modes. In collect mode, activity is implanted onto the tape and moved to the measuring station. In take-away mode, the point of implantation and measuring station coincide and the MTC is used to remove unwanted activity.

Diodes provided at the front of the tape are used to define the section of the focal plane through which ions pass and are implanted on the tape. The MTC can support a three-element Si detector array for pair spectrometry. A subset of CLARION, CLover Array for Radioactive ION beams, consisting of 4 Clover Ge detectors, may be placed in close cross geometry (to date, 2 of the Clovers may be equipped with BGO anti-Compton shields although our near-term plans incorporate two stations able to hold up to 9 Clovers with their BGO shields) with the tape and Si array for beta spectroscopy experiments. A close-up of the present detection station is shown in fig. 12. In two recent experiments of N=Z nuclei, the beta-decay of ^{80}Zr [45] and the decay of two γ-decaying isomers in ^{66}As [46] have been studied. The data are also shown in fig. 12.

3.5 CLARION

The CLover Array for Radioactive ION beams (CLARION) Ge array, nearing completion, includes eleven Clover Ge detectors with BGO anti-Compton shields. Ten of these detectors are segmented for improved Doppler-broadening correction. These detectors, with their segmentation and add-back feature, promise to enhance the detection of weak reaction channels because of their high efficiency ($\geq$150% relative to NaI in add-back mode) and improved resolution despite the high recoil velocities typical of RMS experiments. The total efficiency of the 11 Clover Ge detectors has been measured to be 2.2% at 1.33 MeV. The array has been designed with new CAMAC-based electronics consisting of amplifiers, constant fraction discriminators, four high-resolution 14-bit ADCs, four low-resolution 12-bit ADCs (side channels and BGO energy), and five 12-bit TDCs all in a single, four-slot-wide, module. Included in this package is front-panel readout compatible with FERA standard and computer control of all functions such as thresholds, pole-zero, etc.

By gating the γ rays detected at the target with focal plane detectors, significant enhancements in selectivity can be achieved. As was shown in fig. 10, gating with the energy loss of the recoils in the ionization chamber and simple manipulation of the spectra (portions of spectra subtracted from each other), a "pure" γ ray spectrum may be obtained which contains γ rays which belong only to one nucleus. It is possible to correlate radioactivity events in the DSSD with γ rays detected at the target as is seen in fig. 13. Referred to in the literature as recoil decay tagging (RDT)[10], this technique allows γ-ray spectroscopy to be done beyond the proton drip line. Figure 13 reveals the γ rays assigned to ^{113}Cs, which is a ground state proton emitter with a half life of 18.3(3)μs.

4 Conclusion

The HRIBF Recoil Mass Spectrometer has been commissioned and is now used routinely in experiments. It is performing as expected and is compatible with many detectors. Recent work has concentrated on neutron-deficient nuclei beyond the proton-drip line and along the N=Z line. These studies have enhanced our understanding of the nuclear structure of these nuclei by revealing their decay properties and their excited states.

Operating now for almost three years, the RMS has been instrumented to do the following types of experiments:

1) proton and α radioactivity
2) β-delayed proton decay with Z identification - via X-ray detection
3) recoil-γ with Z identification (ionization chamber and HYBALL)
4) recoil-$\gamma\gamma$
5) recoil decay tagging
6) β, $\beta\gamma$, and e^+e^- pair spectroscopy
7) γ-decaying microsecond-isomer spectroscopy with an extension to isomer decay tagging

Expansion of the operation modes of the RMS may be developed in the future. For example, experiments may be performed at the achromatic focal plane for higher efficiency and shorter time-of-flight. Other types of experiments will become available as new detector systems come on-line and other techniques are developed. The powerful combination of the CLARION, HYBALL, and RMS detection systems will be referred to by the acronym CHARMS.

5 Acknowledgements

This paper is dedicated to the memory of J. D. Garrett. We wish to thank the HRIBF Operations and Facility Support Personnel for their huge contribution to our efforts. We also wish to thank the many HRIBF Users whose data are shown here to illustrate the capabilities of the RMS. The RMS was initiated by Vanderbilt University and the individual elements of the RMS were built by Danfysik A/S. The RMS was funded by the Georgia Institute of Technology, Idaho Nuclear Engineering Laboratory, Louisiana State University, Oak Ridge Associated Universities, Oak Ridge National Laboratory, State of Tennessee, UNISOR, University of Maryland, University of Tennessee, U.S. Department of Energy, and Vanderbilt University. Oak Ridge National Laboratory (ORNL) is managed by Lockheed Martin Energy Research Corp. for the U.S. Department of Energy (DOE) under contract DE-AC05-96OR22464. This research was also supported by DOE through Contract Nos. DE-FG02-96ER40978 (Louisiana State University), DE-AC05-76OR00033 (Oak Ridge Institute for Science and Eduation), DE-FG02-96ER40963 (University of Tennessee), DE-FGO5-87ER40407 (Vanderbilt University), and DE-FG05-87ER40361 (Joint Institute for Heavy Ion Research). The Oak Ridge National Laboratory Postdoctoral Research Associates Program is administered jointly by the Oak

Ridge National Laboratory and the Oak Ridge Institute for Science and Education. The Joint Institute for Heavy Ion Research is supported by its members, the University of Tennessee, Vanderbilt University, and Oak Ridge NAtional Laboratory.

References

[1] D. Rudolph, C. J. Gross, J. A. Sheikh, D. D. Warner, I. G. Bearden, R. A. Cunningham, D. Foltescu, W. Gelletly, F. Hannachi, A. Harder, T. D. Johnson, A. Jungclaus, M. K. Kabadiyski, D. Kast, K. P. Lieb, H. A. Roth, T. Shizuma, J. Simpson, O. Skeppstedt, B. J. Varley, and M. Weiszflog, Phys. Rev. Lett. **76**, (1996) 376.

[2] W. Gelletly, M. A. Bentley, H. G. Price, J. Simpson, C. J. Gross, J. L. Durell, B. J. Varley, Ö. Skeppstedt, and S. Rastikerdar, Phys. Lett. 253B, (1991) 287.

[3] C. J. Gross, D. Rudolph, W. Satula, J. Alexander, C. Baktash, P. J. Coleman-Smith, D. M. Cullen, R. A. Cunningham, J. D. Garrett, W. Gelletly, A. Harder, M. K. Kabadiyski, I. Lazarus, K. P. Lieb, H. A. Roth, D. G. Sarantites, J. A. Sheikh, J. Simpson, O. Skeppstedt, B. J. Varley, and D. D. Warner, Phys. Rev. C **56**, (1997) R591.

[4] S. D. Paul, C. Baktash, W. Satula, C. J. Gross, I. Birrel, R. M. Clark, R. A. Cunningham, M. Devlin, P. Fallon, A. Galindo-Uribarri, T. N. Ginter, D. R. Lafosse, J. Kay, F. Lerma, I.Y. Lee, C. Leyland, A. O. Macchiavelli, B. D. MacDonald, S. J. Metcalfe, A. Piechaczek, D. C. Radford, W. Reviol, L. L. Riedinger, D. Rudolph, K. Rykaczewski, D. G. Sarantites, J. X. Saladin, D. Shapira, G. N. Sylvan, S. L. Tabor, K. S. Toth, W. Weintraub, D. F. Winchell, V. Q. Wood, R. Wyss, and C. H. Yu, Phys. Rev. C **58** (1998) R3037.

[5] P. J. Woods and C. N. Davids, *Annu. Rev. Nucl. Part. Sci.*, **47** (1997) 541 and references therein.

[6] J. C. Batchelder, C. R. Bingham, K. Rykaczewski, K. S. Toth, T. Davinson, J. A. McKenzie, P. J. Woods, T. N. Ginter, C. J. Gross, J. W. McConnell, E. F. Zganjar, J. H. Hamilton, W. B. Walters, C. Baktash, J. Greene, J. F. Mas, W. T. Milner, S. D. Paul, D. Shapira, X. J. Xu, and C. H. Yu Phys. Rev. C **57** (1998) R1042.

[7] C. R. Bingham, J. C. Batchelder, K. Rykaczewski, K. S. Toth, C.-H. Yu, T. N. Ginter, C. J. Gross, R. Grzywacz, M. Karny, S. H. Kim, B. D. MacDonald, J.

Mas, J. W. McConnell, P. B. Semmes, J. Szerypo, W. Weintraub, and E. F. Zganjar, Phys. Rev. C, **59**, (1999) R2984.

[8] K. Rykaczewski, J. C. Batchelder, C. R. Bingham, T. Davinson, T. N. Ginter, C. J. Gross, R. Grzywacz, M. Karny, B. D. MacDonald, J. F. Mas, J. W. McConnell, A. Piechaczek, R. C. Slinger, K. S. Toth, W. B. Walters, P. J. Woods, E. F. Zganjar, B. Barmore, L. Gr. Ixaru, A. T. Kruppa, W. Nazarewicz, M. Rizea, T. Vertse, Phys. Rev. C **60**, (1999) 011301.

[9] A. A. Sonzogni, C. N. Davids, P. J. Woods, D. Seweryniak, M. P. Carpenter, J. J. Ressler, J. Schwartz, J. Uusitalo, and W. B. Walters, Phys. Rev. Lett., **83**, (1999) 1116.

[10] E. S. Paul, P. J. Woods, T. Davinson, R. D. Page, P. J. Sellin, C. W. Beausang, R. M. Clark, R. A. Cunningham, S. A. Forbes, D. B. Fossan, A. Gizon, J. Gizon, K. Hauschild, I. M. Hibbert, A. N. James, D. R. LaFosse, I. Lazarus, H. Schnare, J. Simpson, R. Wadsworth, and M. P. Waring, Phys. Rev. C **51** (1995) 78.

[11] D. Seweryniak, C. N. Davids, W. B. Walters, P. J. Woods, I. Ahmad, H. Amro, D. J. Blumenthal, L. T. Brown, M. P. Carpenter, T. Davinson, S. M. Fischer, D. J. Henderson, R. V. F. Janssens, T. L. Khoo, I. Hibbert, R. J. Irvine, C. J. Lister, J. A. MacKenzie, D. Nisius, C. Parry, and R. Wadsworth, Phys. Rev. C **55** (1997) R2137.

[12] C. J. Gross, Y. A. Akovali, C. Baktash, J. C. Batchelder, C. R. Bingham, M. P. Carpenter, C. N. Davids, T. Davinson, D. Ellis, A. Galindo-Uribarri, T. N. Ginter, R. Grzywacz, R. V. F. Janssens, J. W. Johnson, J. F. Liang, C. J. Lister, J. Mas, B. D. MacDonald, S. D. Paul, A. Piechaczek, D. C. Radford, W. Reviol, K. Rykaczewski, D. Shapira, K. S. Toth, W. Weintraub, P. J. Woods, C. H. Yu, E. F. Zganjar, and J. Uusitalo, in AIP Conference Proceedings Vol 455, edited by B. M. Sherrill, D. J. Morrissey, and C. N. Davids, (AIP Press, New York, 1998) p. 444.

[13] C.-H. Yu, J. C. Batchelder, C. R. Bingham, R. Grzywacz, K. Rykaczewski, K. S. Toth, Y. A. Akovali, C. Baktash, A. Galindo-Uribarri, T. N. Ginter, C. J. Gross, M. KArny, S. H. Kim, B. D. MacDonald, S. D. Paul, D. C. Radford, J. Szerypo, and W. Weintraub, Phys. Rev. C **58** (1998) R3042.

[14] E. Maglione, L. S. Ferreira, and R. J. Liotta, Phys. Rev. Lett. **81**, (1998) 538.

[15] S. Aberg, P. B. Semmes, and W. Nazarewicz, Phys. Rev. C, **56**, (1997) 1762.

[16] S. G. Frauendorf and J. A. Sheikh, Nucl. Phys. **645A**, (1999) 509.

[17] J. Engel, K. Langanke, and P. Vogel, Phys. Lett. **389B**, (1996) 211.

[18] D. J. Dean, S. E. Koonin, K. Langanke, P. B. Radha, and Y. Alhassid, Phys. Rev. Lett. **74**, (1995) 2909.

[19] A. Petrovici, K. W. Schmidt, and A. Faessler, Nucl. Phys. **A571** (1999) 197.

[20] T. M. Cormier, M. G. Herman, B. S. Lin, and P. M. Stwertka, Nucl. Instrum. Methods **212** (1983) 185.

[21] A. N. James, T. P. Morrison, K. L. Ying, K. A. Connell, H. G. Price, and J. Simpson, Nucl. Instrum. Methods Phys. Res. Sect. **A267** (1988) 144.

[22] C. N. Davids, B. B. Back, K. Bindra, D. J. Henderson, W. Kutschera, T. Lauritsen, Y. Nagame, P. Sugathan, A. V. Ramayya, and W. B. Walters, Nucl. Instrum. Methods in Phys. Res. **B70** (1992) 358.

[23] C. Signorini, S. Beghini, A. Dal Bello, G. Montagnoli, F. Scarlassara, G. F. Segato, F. Soramel, D. Ackermann, L. Corradi, A. Facco, H. Moreno, L. Müller, D. R. Napoli, and G. F. Prete, Nucl. Instrum. Methods **A339** (1994) 531.

[24] A.K. Sinha, N. Madhavan, J.J. Das, P. Sugathan, D.O. Kataria, A.P. Patro, and G.K. Mehta, Nucl. Instrum. Methods Phys. Res. A **339**, (1994) 543.

[25] P. J. Sellin, P. J. Woods, D. Branford, T. Davinson, N. J. Davis, D. G. Ireland, K. Livingston, R. D. Page, A. C. Shotter, S. Hofmann, R. A. Hunt, A. N. James, M. A. C. Hotchkis, M. A. Freer, and S. L. Thomas, Nucl. Instrum. Methods A **311**, (1992) 217.

[26] D. Bazzacco for the GASP Collaboration, *International Conf. on Nuclear Structure at High Angular Momentum and Workshop on Large Gamma-Ray Detector Arrays*, AECL-10613, Vol. 2, p376, 1992.

[27] C.W. Beausang, S. A. Forbes, P. Fallon, P. J. Nolan, P. J. Twin, J. N. Mo, J. C. Lisle, M. A. Bentley, J. Simpson, F. A. Beck, D. Curien, G. deFrance, G. Duchene, and P. Popescu, Nucl. Instrum. Methods Phys. Res. Sect. **A313**, 37 (1992).

[28] I. -Y. Lee, Nucl. Phys. **A520**, (1990) 641c.

[29] D. G. Sarantites, P. F. Hua, M. Devlin, L. G. Sobotka, J. Elson, J. T. Hood, D. R. LaFosse, J. E. Sarantites, and M. R. Maier, Nucl. Instrum. Methods Phys. Res., Sect. A **381** (1996) 418.

[30] A. Galindo-Uribarri, Prog. Part. Nucl. Phys. **28**, (1992) 463.

[31] J. D. Cole, T. M. Cormier, J. H. Hamilton, and A. V. Ramayya, Nucl. Instrum. Methods in Phys. Res. **B70** (1992) 343.

[32] J. D. Cole, T. M. Cormier, and J. H. Hamilton, in *Exotic Nuclear Spectroscopy*, edited by C. McHarris, (Plenum Press, New York, 1990) p. 11.

[33] P. F. Mantica, Nucl. Instrum. Methods in Phys. Res. **B99** (1995) 338.

[34] C. J. Gross, T. N. Ginter, Y. A. Akovali, M. J. Brinkman, J. W. Johnson, J. Mas, J. W. McConnell, W. T. Milner, D. Shapira, and A. N. James, in *Application of Accelerators in Research and Industry*, edited by J. L. Duggan and I. L. Morgan, (AIP Press, New York, 1997) p. 401.

[35] T. N. Ginter, in *Perspectives in Nuclear Physics*, edited by J. H. Hamilton, H. K. Carter, and R. B. Piercey, (World Scientific, Singapore, 1999) p. 139.

[36] R. Tribble, J. Bronson, H. Dejbakhsh, C. Gagliardi, S. Hale, W. Lui, D. Semon, H. Xu, S. Yennello, and X. Zhou, Texas A&M Progress Report 1992-1993, p. V-136.

[37] H. Wollnik, J. Brezina, and M. Berz, Nucl. Instrum. and Meth. **A258**, (1987) 402.

[38] T.M. Cormier, P.M. Stwertka, M. Herman, and N.G. Nicolis, Phys. Rev. C **30**, (1984) 1953.

[39] K. E. Rehm, M. Paul, J. Gehring, B. Glagola, D. Henderson, W. Kutschera, A. H. Wuosmaa, Nucl. Instrum. Methods in Phys. Res. **A344**, (1994) 614.

[40] A. N. James, K. A. Connell, and R. A. Cunningham, Nucl. Instrum. Methods in Phys. Res. **B53**, (1991) 349.

[41] E. S. Paul, A. J. Boston, A. Galindo-Uribarri, T. N. Ginter, C. J. Gross, A. N. James, P. J. Nolan, R. D. Page, S. D. Paul, A. Piechaczek, D. C. Radford, W. Reviol, L. L. Riedinger, H. C. Scraggs, W. Weintraub, and C. H. Yu, Phys. Rev. C **58**, (1998) 801.

[42] S. L. Thomas, T. Davinson, and A. C. Shotter, Nucl. Instrum. Methods in Phys. Res. **A288**, (1990) 212.

[43] T. Davinson, A. C. Shotter, E. W. MacDonald, P. Jobanputra, A. J. Stephens, and S. L. Thomas, Nucl. Instrum. Methods in Phys. Res. **A288**, (1990) 245.

[44] E. F. Zganjar, A. Piechaczek, J. C. Batchelder, and C. J. Gross, in *Perspectives in Nuclear Physics*, edited by J. H. Hamilton, H. K. Carter, and R. B. Piercey, (World Scientific, Singapore, 1999) p. 187.

[45] J. J. Ressler, A. Piechaczek, W. B. Walters, A. Aprahamian, M. Wiescher, J. C. Batchelder, C. R. Bingham, D. S. Brenner, T. N. Ginter, C. J. Gross, R. Grzywacz, D. Kulp, B. D. MacDonald, W. Reviol, J. Rikovska, K. Rykaczewski, J. A. Winger, and E. F. Zganjar, Phys. Rev. Lett., submitted.

[46] A. Piechaczek, A. Aprahamian, J. C. Batchelder, C. R. Bingham, D. Brenner, C. J. Gross, T. N. Ginter, R. Grzywacz, B. D. MacDonald, W. D. Kulp, S. D. Paul, J. J. Ressler, W. Reviol, K. Rykaczewski, R. Terry, K. S. Toth, W. B. Walters, J. A. Winger, J. L. Wood, and E. F. Zganjar, in *Perspectives in Nuclear Physics*, edited by J. H. Hamilton, H. K. Carter, and R. B. Piercey, (World Scientific, Singapore, 1999) p. 201.

Table 1
Summary of the knobs available for adjusting the tune of the RMS and the elements they change. Elements which are weakly affected by a knob setting are listed in parentheses.

Knob	Function	Affected Elements
1	mass resolution	Q4, Q5
2	vertical transmission through momentum achromatic focus	Q1, Q2
3	second order correction ($x/\theta\delta E$)	S1, S2
4	second order correction ($x/\delta E\delta E$)	S1, S2
5	target-Q1 distance	Q1, Q2
6	mass dispersion ($x/\delta m$)	Q6, Q7, (Q4), (Q5)
7	vertical focus	Q6, Q7, (Q4), (Q5)
8	vertical transmission through mass separator	Q4, Q5, Q6, Q7

Table 2
Detectors systems compatible with the RMS

Device/Detector	Purpose
Position Sensitive Avalanche Counter (PSAC)	Recoil position (A/Q)
Double-sided Silicon Strip Detector (DSSD)	Charged-particle radioactivity
Ionization Chamber (IC)	Z identification
Moving Tape Collector (MTC)	Beta radioactivity and transport
CLover Array for Radioactive ION Beams (CLARION)	Gamma-rays
Subset of CLARION at final focal plane	Gamma-rays
Large area X-ray detector (LOAX)	X-rays
Large area silicon detectors	Charged-particle and beta radioactivity
HYBALL (now being commissioned)	Charged-particle detection

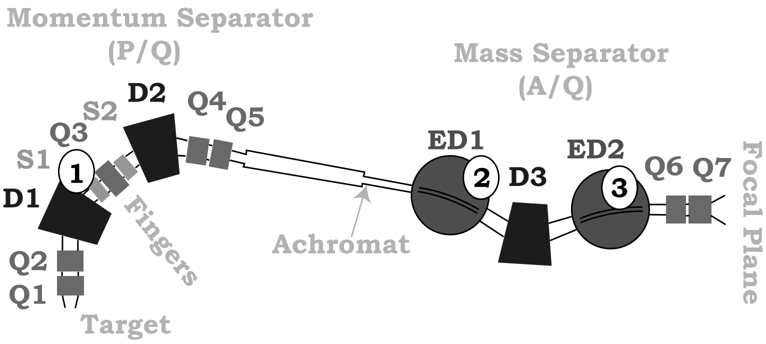

Fig. 1. A schematic of the RMS. Areas (1) and (3) are the places where the primary beam is usually deposited inside the RMS. Areas (2) and (3) are places where the beam is deposited in similar mass spectrometers which do not have a momentum separator. The RMS achieves superior beam rejection by moving the first beam-dump away from the final focal plane. Beam is deposited in area (3) only when the kinematic properties of the beam are similar to those of the products of interest. In these cases, the fingers may be used to intercept the beam and prevent its transport to area (3).

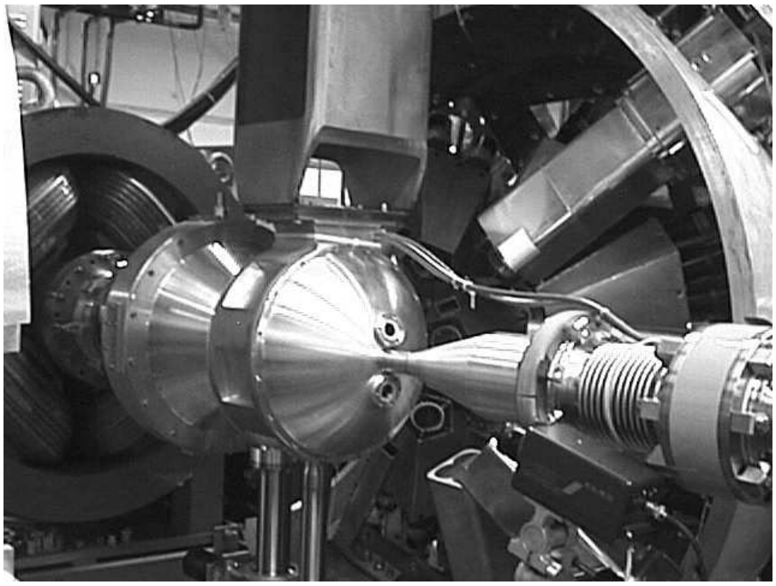

Fig. 2. The target chamber of the RMS. The target is approximately 75 cm from the first quadrupole of the RMS. Note the large fantail in the forward section of the chamber. This 30 cm extension allows most of the scattered radioactive primary beam to be dumped away from the center of the CLARION Ge detector array. The 14 cm radius chamber will hold a 95-element CsI charged-particle detector array HYBALL and silicon strip detectors in the fantail. The two appendages below the chamber are transfer tubes for changing targets and charge-reset foils without letting the entire chamber up to air.

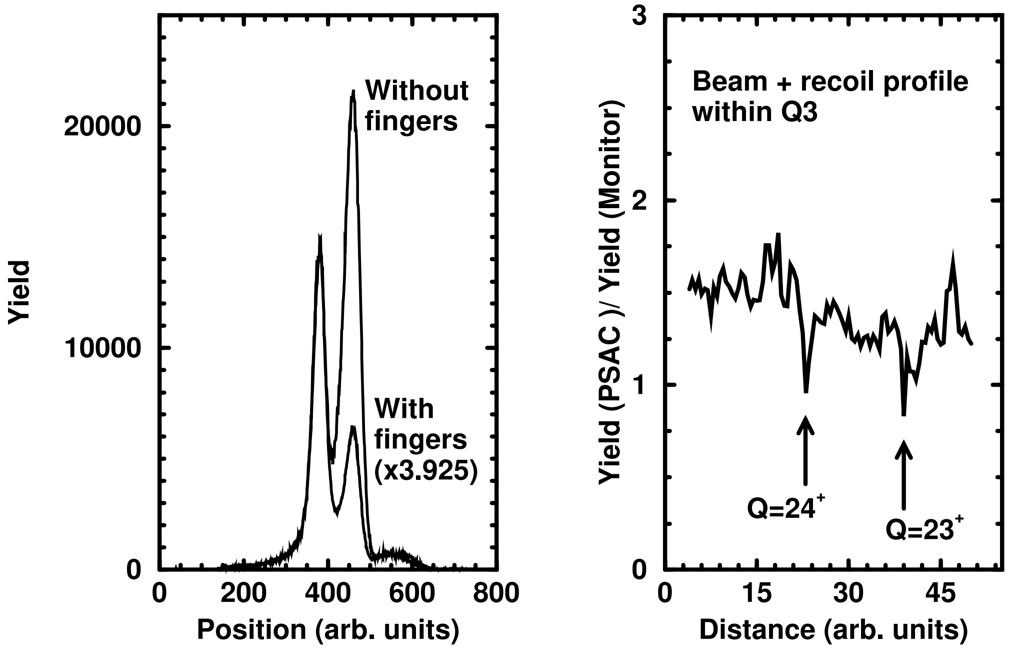

Fig. 3. *(Right)* Profile of ions as determined by countrate at the achromatic focus as a function of position of one finger inside Q3. Two drops in rate are marked and correspond to primary beam which has been stripped at the target to charge states (Q) 23 and 24. *(Left)* A comparison of the normalized yield (with respect to Q=23) of primary beam of Q=24 at the achromatic focus with and without 3 fingers in place. The reduction in rate suggests that a factor of 3 reduction in primary beam transmission to the achromatic focus may be achieved. The data were taken with a 220 MeV ^{58}Ni beam passing through a ^{nat}C target of thickness 150 μg/cm^2 to produce ions with a range of charge states.

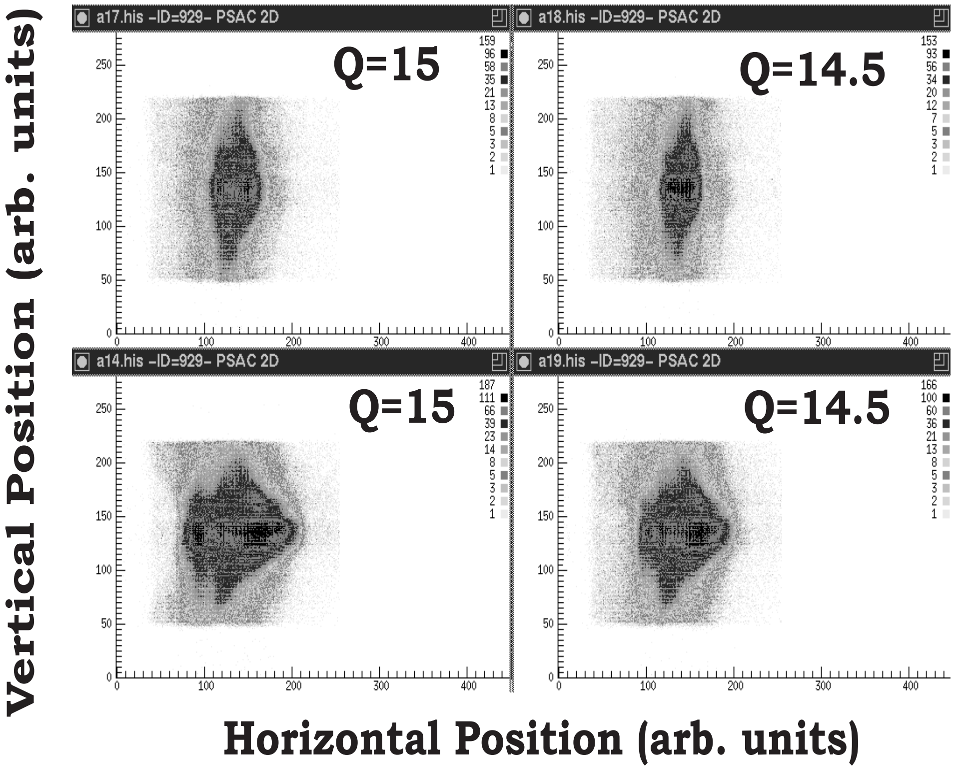

Fig. 4. The two-dimensional spatial image of ions at the achromatic focal plane of the RMS using a beam of 85.3 MeV ^{28}Si ions and a ^{54}Fe target. The RMS was tuned for A=79 recoils at 24 MeV with Q=15 and Q=14.5. The spectra on the top are the images when the RMS is tuned to transmit ions to the final focal plane. The spectra on the bottom are the images produced with vertical-focussing quadrupole Q5 strengthened by 3.5%. The vertical bar becomes more circular under these conditions and better fits the square profile of the DSSD.

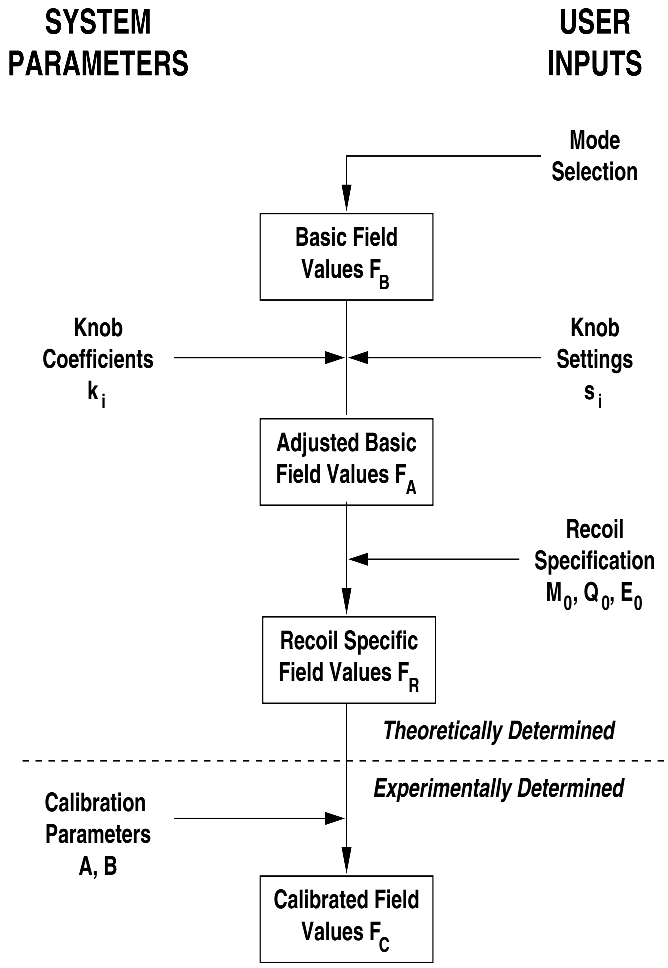

Fig. 5. Flow diagram of the RMS control system. A user needs only to input the mode, knob values, mass (M), energy (E), and charge state (Q) of the ion into the control system.

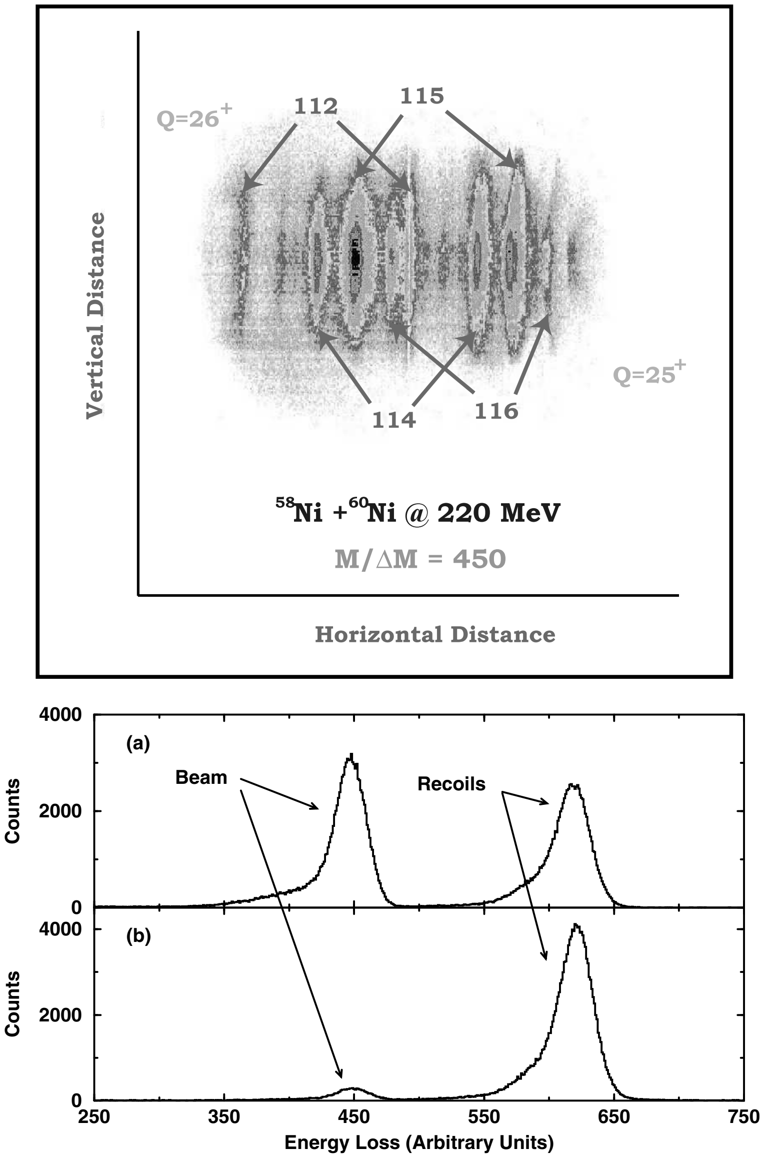

Fig. 6. *(Top)* The two-dimensional image of the focal plane of the RMS in the ^{58}Ni + ^{60}Ni reaction. The mass resolution was measured to be $M/\Delta M = 450$. Note that this spectrum was taken in "singles" requiring coincidences only between the anode and the position signals. Very little primary beam is transmitted through the RMS. *(Bottom)* The energy-loss spectra from an ionization chamber at the final focal plane by using the inverse kinematic reaction ^{58}Ni + ^{28}Si at 208 MeV. The 400 μg/cm^2 target was supported by a 900 μg/cm^2 Ta foil which faced the beam. (a) The data taken with only the PSAC as trigger *ie.*, all ions transmitted to the focal plane. (b) Data taken as in (a) but with the additional requirement that a γ ray is detected at the target, effectively adding a time correlation condition. The total amount of beam reaching the focal plane was approximately 56% of the total events. These "uninteresting" events were further suppressed to 7% of the data by requiring the detection of a γ ray.

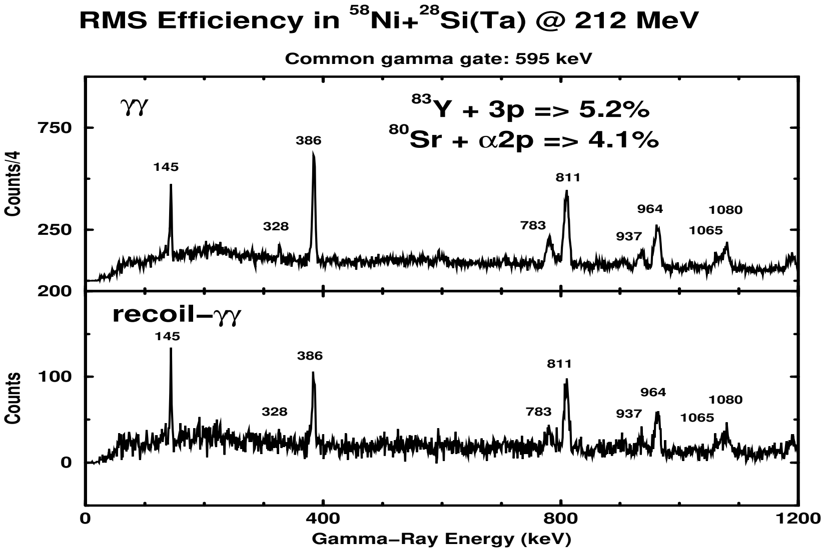

Fig. 7. Two one-dimensional 595-keV gamma-gated spectra where the lower spectrum is also gated by the PSAC. The difference in yield for the 3p and α2p evaporation channels between the mass gated and non-mass gated spectrum establishes the efficiency of the RMS, which is clearly reaction and channel dependent. See text for discussion on the efficiency of recoil mass spectrometers. Deadtime corrections were made in hardware by electronically reducing the pure $\gamma\gamma$ coincidence rate by a factor of 4 to match the recoil-$\gamma\gamma$ coincidence rate. The reaction used was ^{58}Ni at 212 MeV on a ^{28}Si target of 400 μg/cm^2 with a 900 μg/cm^2 Ta front.

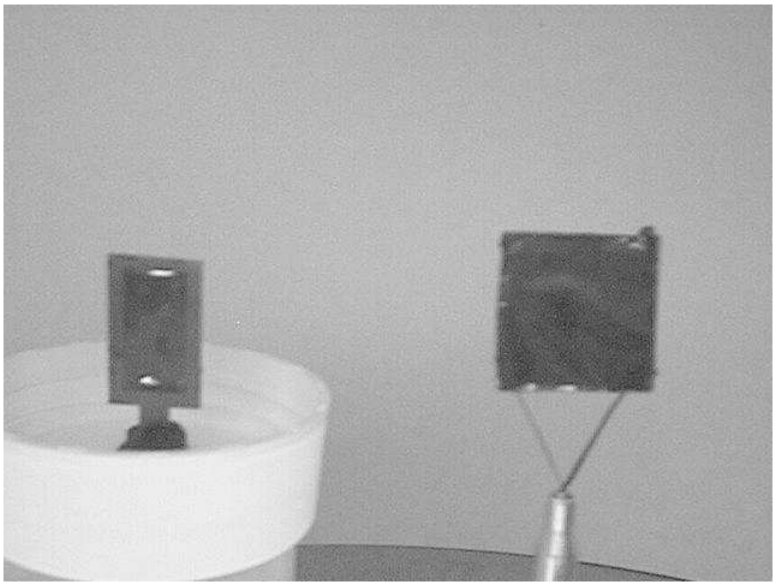

Fig. 8. A photograph of charge reset foils mounted on two different frames. The rectangular frame on the left has sides of approximately 3 mm in width. The square frame on the right has a small cross-section to the beam to minimize the shielding of detectors in the forward section of the target chamber and to minimize the deposition of scattered radioactive beam ions near the center of CLARION.

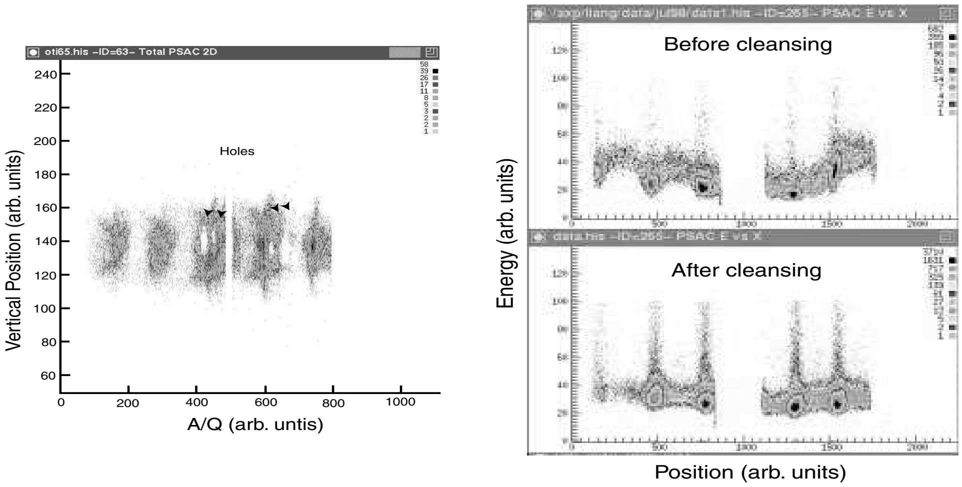

Fig. 9. The two dimensional position spectrum of the focal plane of the RMS with "holes" is on the left. Energy vs position spectra (taken with the HRIBF Enge spectrometer) are on the right. Note the non-uniform energy gains as a function of position. Cleansing the wires can make these planes useable again.

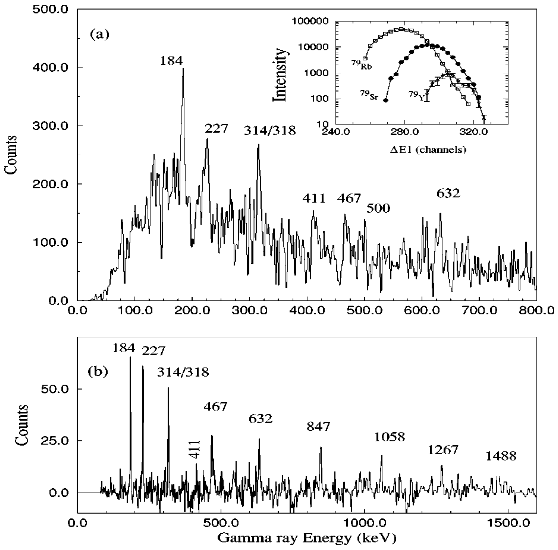

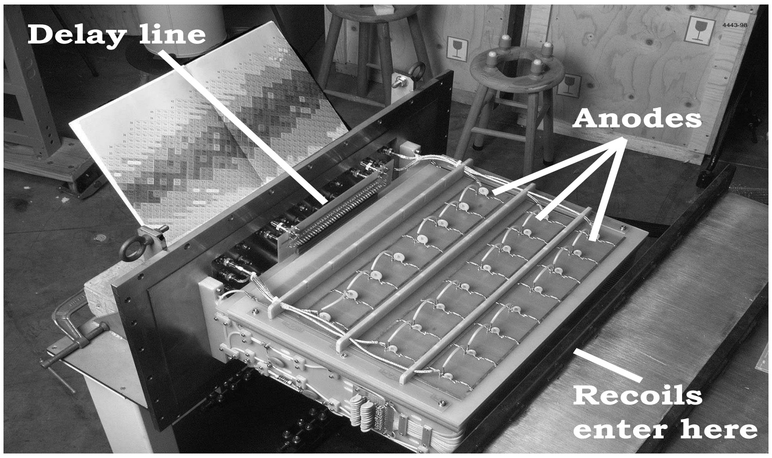

Fig. 10. *(Top)* The one-dimensional "pure" ^{79}Y spectrum gated by mass and energy loss in the ionization chamber. The data were taken with six Clover Ge detectors from the CLARION array without Compton-suppression. The inset shows the γ-ray yield as a function of energy loss for selected transitions from A=79 and Z=37,38,39 isotopes. The lower panel is data from GAMMASPHERE gated on transitions assigned to ^{79}Y following identification at the RMS. *(Bottom)* A picture of the top of the ionization chamber.

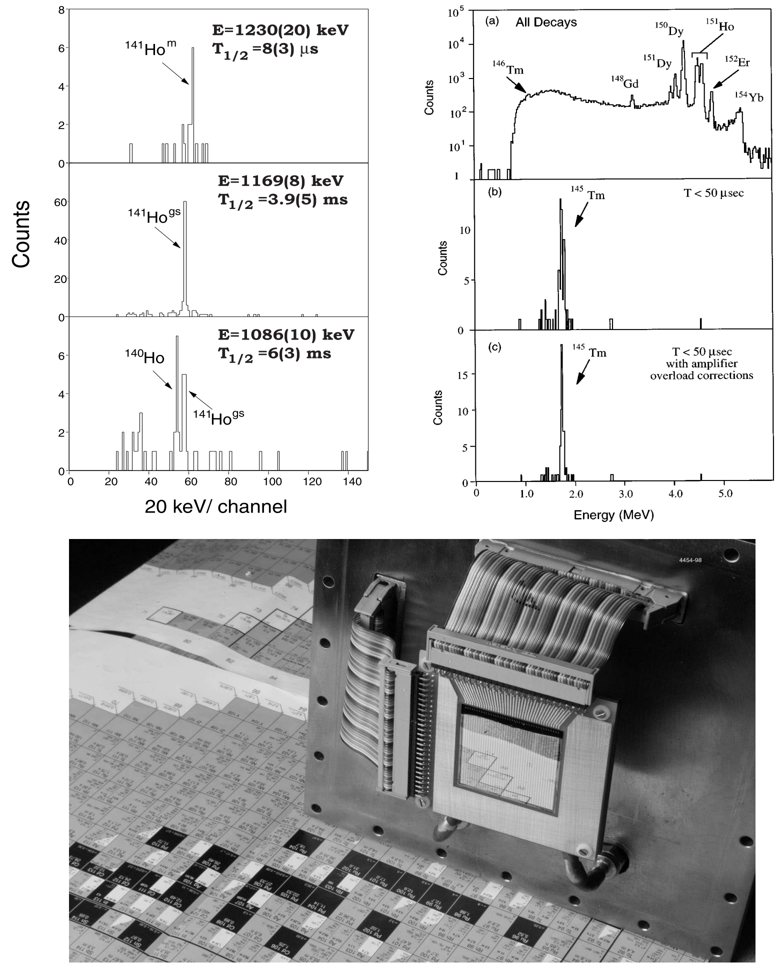

Fig. 11. *(Top left)* Mass- and time-gated, one-dimensional, decay spectra from the DSSD in the reactions ^{92}Mo(^{54}Fe,p4n)^{141}Ho and ^{92}Mo(^{54}Fe,**p5n**)^{140}Ho at 315 MeV. *(Top right)* Same as above but for the reaction ^{92}Mo(^{58}Ni,p4n)^{145}Tm at 315 MeV. The other masses result from the isotopic contaminants (primarily ^{98}Mo) in the target. *(Bottom)* Photograph of the 40 strip by 40 strip DSSD (40 mm x 40 mm) mounted on the back plate of a chamber. A new chamber incorporating a DSSD-Si-Si telescope and kevlar window is now in use.

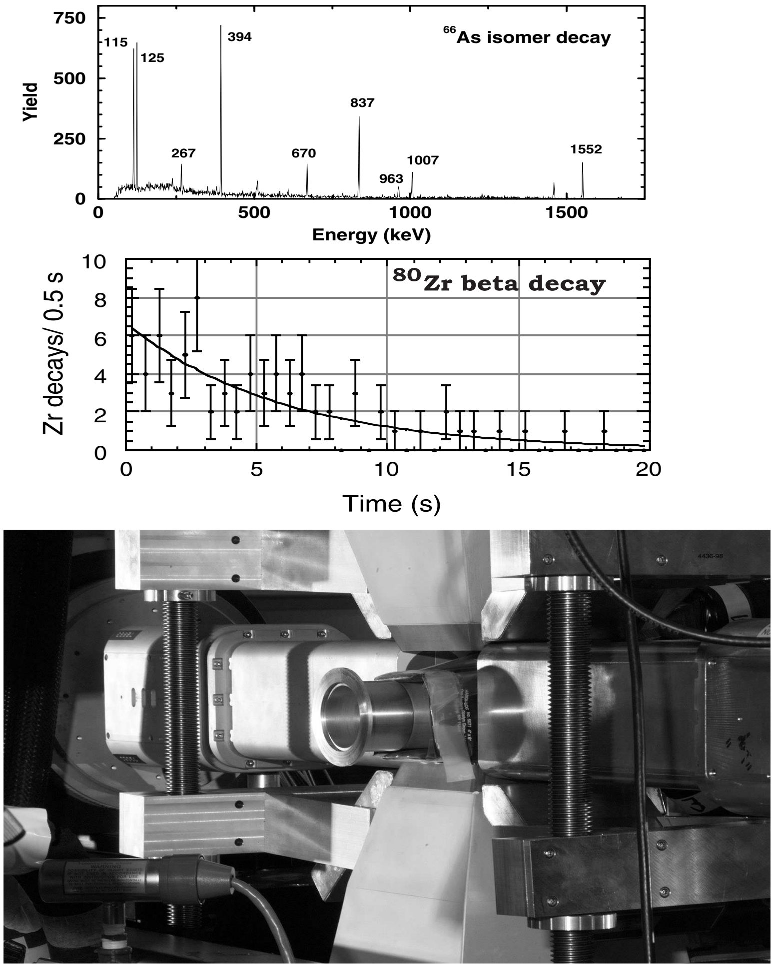

Fig. 12. *(Top)* Time-gated γ-ray spectrum revealing the decay of microsecond-isomers in the odd-odd, N=Z nucleus ^{66}As. The decays, observed at the RMS focal plane with four Clover Ge detectors, were correlated with a recoil signal from the PSAC. The data were taken with the reaction ^{40}Ca(^{28}Si,pn)^{66}As at 95 MeV. The MTC was operated in take-away mode reducing contamination from longer-lived β-decay products. *(Middle)* The background-corrected, β-decay halflife data of the self-conjugate nucleus ^{80}Zr. The data were obtained by detecting the 84 keV transition in ^{80}Y which depopulates a 4 μs isomer. A total of 87 events, 11 of which were taken as background, were collected. The solid line represents a 4.1 s halflife. The MTC was operated in collect mode. *(Bottom)* The MTC counting station surrounded by four clover Ge detectors from the CLARION array. Two detectors are BGO Compton-suppressed. The MTC (behind the Ge detectors) can transport activities to or from this station depending on the half-life of the species being studied. An array of three 5-mm thick Si detectors for conversion electron spectroscopy may also be used at this station. This system is very flexible as it uses 160 mm quick-connect clamp flanges so that different configurations are possible.

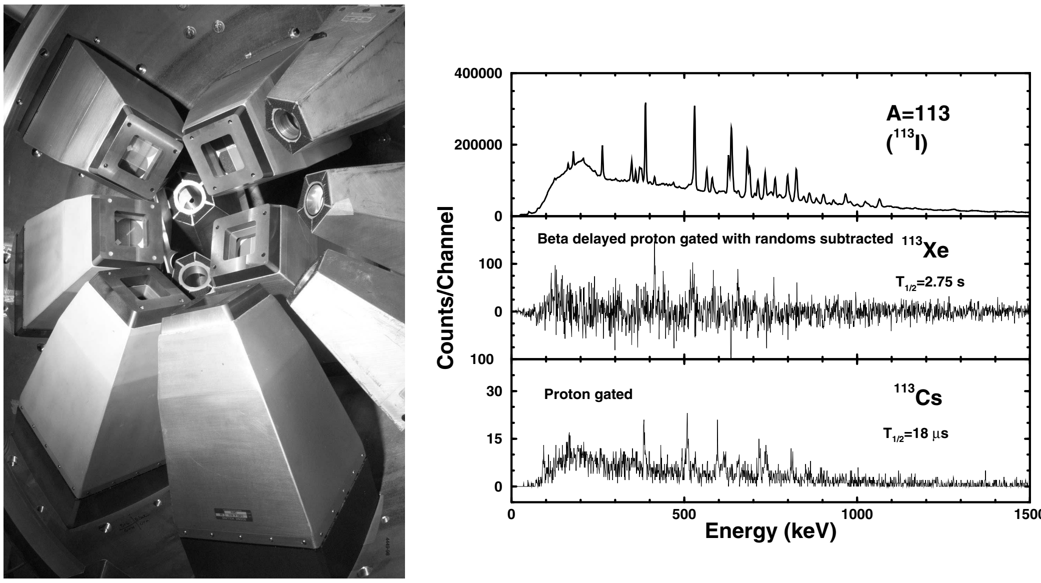

Fig. 13. *(Left)* Photograph of six clover Ge detectors and five coaxial single-crystal Ge detectors of one-hemisphere of the CLARION array at the RMS. Comprised of a total of 11 Clover and up to 11 duet Ge detectors, the absolute photopeak efficiency of the system at 1.3 MeV is approximately 3.5%. *(Right)* Mass 113 gated γ-ray spectra taken with an early implementation of the CLARION Ge array. The data were taken in the reaction ^{58}Ni + ^{58}Ni at 230 MeV. Recoils were implanted into a DSSD and those which emitted protons by ground state radioactivity (^{113}Cs) and β-delayed protons (^{113}Xe) were detected and correlated with γ-rays emitted at the target position. The more prevalent pure β-decay events were not observed in the DSSD and these nuclei, primarily ^{113}I, dominate the top spectrum. A portion of the top spectrum was subtracted from the beta-delayed proton gated spectrum to approximate a random background. No subtraction was necessary to produce the ^{113}Cs spectrum.